1-1-1978

Thermal Properties and MlcroBtructurc of a Bonded Silicon Carbide Refractory.

Eric John Minford

Thermal Properties and Microstructure of a Bonded Silicon Carbide Refractory

by

Eric John Minford

A Thesis

Presented to the Graduate Committee

of Lehigh University

in Candidacy for the Degree of

Master of Science

in

Metallurgy and Materials Engineering

Lehigh University

1978

Certificate of Approval

This thesis is accepted in partial fulfillment of the requirements for the degree of Master of Science.

8/31/79
(Date)

Professor in Charge

Chairman of Department

THERMAL PROPERTIES AND MICROSTRUCTURE OF A BONDED SILICON CARBIDE REFRACTORY

Eric J. Minford

The effects of high temperature service in a zinc retort on the thermal properties and microstructure of a silicon carbide refractory body were determined. Samples in the 'as-received' condition as well as samples taken from bricks after three years of continuous service were examined. Thermal diffusivity of the samples was measured by the laser-flash technique. The 'as-received' samples exhibited values of thermal diffusivity 20 to 30 percent lower across a broad temperature range than the samples which were in service. The linear thermal expansion was measured on an automatic dilatometer. The coefficient of thermal expansion of the 'as-received' samples was measured to be 15 to 20 percent higher than the samples which had been in service. X-ray diffraction analysis showed the bonding matrix of the 'as-received' samples to be multi-phase, composed of α-and β-Si_3N_4 and Si_2N_2O. The diffraction analysis of the three year service samples showed their matrix to be composed primarily of Si_2N_2O with some α-and β-Si_3N_4 present. Scanning electron microscopy was used to examine fracture surfaces of the samples. The bonding matrix of the 'as-received' samples appeared to have grains of two distinct morphologies; the three year service samples exhibited grains of only one

of these forms. Optical microscopy and grain size distribution analysis show the silicon carbide grains to be very stable. The average grain size of the sample from the inside face of the retort wall was slightly higher than that of the 'as-received' sample. The average grain size of the outside face sample was lower than that of the 'as-received' sample. The three year service samples appear to be much less porous than the 'as-received' samples.

Acknowledgements

The author wishes to thank Dr. S. R. Butler for his guidance and advice during the course of this investigation.

Appreciation is extended to Dr. S. K. Tarby and the Chemical Metallurgy section for funding of this work. The author also wishes to extend gratitude to Richard Leidich, Doug Bush and Gene Kozma for helping to keep all the equipment in good working condition.

The author wishes also to thank his fellow graduate students in the Metallurgy and Materials Engineering Department as well as the Faculty and Staff of that department and the Fairchild Center for Solid State Studies, The Materials Research Center, and the Physics Department.

Finally, the author wishes to thank his parents, Mr. and Mrs. Jack H. Minford for their understanding and encouragement throughout the course of his education. The author also thanks his loving wife, Toni, for her love, understanding, support and devotion.

Table of Contents

	Page
Certificate of Approval	ii
Acknowledgements	iii
Table of Contents	iv
Lists of Figures	vi
Lists of Tables	viii
Abstract	1
I. Introduction and Statement of the Problem	3
II. Literature Review	
Silicon Carbide History and Processing	5
Thermal Diffusivity	9
III. Experimental Procedures	
Material	14
Characterization	
1. X-ray Diffraction	14
2. Thermal Expansion	16
3. Scanning Electron Microscopy	16
4. Optical Microscopy and Grain Size Distribution Analysis	17
Thermal Diffusivity versus Temperature	17
IV. Results	
Characterization	
1. X-ray Diffraction	19
2. Thermal Expansion	19
3. Scanning Electron Microscopy	19
4. Optical Microscopy and Grain Size Distribution Analysis	34
Thermal Diffusivity versus Temperature	43
V. Discussion	48
VI. Summary and Conclusions	52
References	54

	Page
Appendix A - Experimental Configuration and Allignment	56
Appendix B - Thermocouple Measurement Technique and System Sensitivity	59
Appendix C - Data from Grain Size Distribution Analysis	64
Vita	67

List of Figures

No.	Title	Page
1	Thermal Expansion of Sample NA	21
2	Thermal Expansion of Sample NG-I	22
3	Thermal Expansion of Sample NG-M	23
4	Thermal Expansion of Sample NG-O	24
5	Scanning Electron Photomicrograph of Sample NA	26
6	Scanning Electron Photomicrograph of Sample NA	27
7	Scanning Electron Photomicrograph of Sample NG-I	28
8	Scanning Electron Photomicrograph of Sample NG-I	29
9	Scanning Electron Photomicrograph of Sample NG-M	30
10	Scanning Electron Photomicrograph of Sample NG-M	31
11	Scanning Electron Photomicrograph of Sample NG-O	32
12	Scanning Electron Photomicrograph of Sample NG-O	33
13	Optical Photomicrograph of Sample NA	35
14	Optical Photomicrograph of Sample NG-I	36
15	Optical Photomicrograph of Sample NG-M	37
16	Optical Photomicrograph of Sample NG-O	38
17	Grain Size Distribution of Sample NA	39
18	Grain Size Distribution of Sample NG-I	40
19	Grain Size Distribution of Sample NG-M	41
20	Grain Size Distribution of Sample NG-O	42

No.	Title	Page
21	Variation of Thermal Diffusivity with Temperature for Sample NA	44
22	Variation of Thermal Diffusivity with Temperature for Sample NG-I	45
23	Variation of Thermal Diffusivity with Temperature for Sample NG-M	46
24	Variation of Thermal Diffusivity with Temperature for Sample NG-O	47
25	Optical Photomicrograph of Outer Surface of Refractory	50
A1	Schematic Diagram of Experimental Apparatus	57
B1	Variation of Thermal Diffusivity with Temperature of 1023 Steel Measured by Different Detection Techniques	60
B2	Variation of Thermal Diffusivity with Temperature of (MnZn)Fe_2O_4 Measured by Different Detection Techniques	61

List of Tables

No.	Title	Page
I	Chemical Composition and Properties of 'As-received' Samples	15
II	X-ray Diffraction Results	20
III	Calculated Mean Linear Thermal Expansion Coefficients	25
IV	Calculated Average Grain Sizes	25
CI	Grain Size Distribution Analysis Data for Sample NA	65
CII	Grain Size Distribution Analysis Data for Sample NG-I	65
CIII	Grain Size Distribution Analysis Data for Sample NG-M	66
CIV	Grain Size Distribution Analysis Data for Sample NG-O	66

ABSTRACT

The effects of high temperature service in a zinc retort on the thermal properties and microstructure of a silicon carbide refractory body were determined. Samples in the 'as-received' condition as well as samples taken from bricks after three years of continuous service were examined. Thermal diffusivity of the samples was measured by the laser-flash technique. The 'as-received' samples exhibited values of thermal diffusivity 20 to 30 percent lower across a broad temperature range than the samples which were in service. The linear thermal expansion was measured on an automatic dilatometer. The coefficient of thermal expansion of the 'as-received' samples was measured to be 15 to 20 percent higher than the samples which had been in service. X-ray diffraction analysis showed the bonding matrix of the 'as-received' samples to be multi-phase, composed of α-and β-Si_3N_4 and Si_2N_2O. The diffraction analysis of the three year service samples showed their matrix to be composed primarily of Si_2N_2O with some α-and β-Si_3N_4 present. Scanning electron mixroscopy was used to examine fracture surfaces of the samples. The bonding matrix of the 'as-received' samples appeared to have grains of two distinct morphologies; the three year service samples exhibited grains of only one of these forms. Optical microscopy and grain size

distribution analysis show the silicon carbide grains to be very stable. The average grain size of the sample from the inside face of the retort wall was slightly higher than that of the 'as-received' sample. The average grain size of the outside face sample was lower than that of the 'as-received' sample. The three year service samples appear to be much less porous than the 'as-received' samples.

I. Introduction and Statement of the Problem

Silicon carbide has been manufactured for over 85 years. Initially its primary uses were in gem cutting and abrasive applications; however, soon after nineteen hundred, the refractory properties of silicon carbide became important. Since then the applications of silicon carbide refractories have steadily increased. Uses of silicon carbide refractory shapes include kiln furniture, retorts, and condensers in zinc refining[1], furnace muffles, gas scrubbers, recuperators, reheating furnace skid rails, slag-lines of coal-fired boilers, blast furnace downcomer elbows, dust collectors, coke shute lines, blast furnace wear plate, blast furnace splash-plate, troughs, runners, cinder notches, and open-hearth roofs in the steel industry[2], and linings for aluminum reduction cells[3]. Other special applications include use as rocket nozzles, turbine blades, brazing jigs, and many others.

In 1929 the New Jersey Zinc Company began using a vertical retort process for the distillation of zinc vapor from oxide ores[4]. The feasibility of this process was dependent on the excellent thermal conductivity, good hot strength, and resistance to attack by zinc liquid and vapor of silicon carbide refractory shapes. These vertical retorts are operated contin-

uously at temperatures in the range of 1300 to 1600K for several years.

The purpose of this study was to determine the effect of high temperature service in a zinc retort on the thermal properties and microstructure of a silicon carbide refractory body. 'As-received' samples and samples taken from bricks after three years of service have been examined. The thermal properties of interest, thermal diffusivity and thermal expansion were measured as a function of temperature up to the service temperature range. The microstructure was characterized by optical and scanning electron microscopy. Phase identification was made by x-ray powder diffraction analysis.

II. Literature Review

Silicon Carbide History and Processing

For many years silicon carbide has been used for abrasives, refractories, and heating elements because of its unique properties prominent for these applications, including high hardness, excellent thermal stability and good high temperature electrical conductivity. The silicon carbide generally used is a combination of several of the alpha and the beta crystallographic forms. The beta phase has a cubic sphalerite structure, while the alpha polytypes, of which there have been 70 identified, have hexagonal layer structures characterized by different stacking sequences of a 'wurtzite-like' structure[5]. Beta silicon carbide is the low temperature form, stable to approximately 2400K, where it transforms to one of the alpha forms.

Commercially, silicon carbide is usually manufactured by packing silica and carbon around a graphite resistor and heating to cause the reaction:

$$SiO_2+3C \rightarrow SiC+2CO$$

Other methods for producing silicon carbide include substitution silicon for silica to avoid the need for additional carbon, use of a 'hot wire' process to reduce volatile silicon halides in hydrogen, adding

carbon to a molten high-silicon alloy, and reacting molten or vaporized silicon with carbon. Using the reacted silicon carbide grain, refractory body production began with the use of bonding agents. The first bonding material for silicon carbide refractories was a mixture of minerals and clays which formed silicates during firing. These wares have become widely accepted for good strength, oxidation resistance, heat conduction, and ability to withstand wear and corrosion. As would be expected, the refractories are severly limited by the softening of the silicate bonds in the range of 1750-1850K.

According to Butler[1], the first major breakthrough in silicon carbide refractory technology occurred with the utilization of silicon nitride instead of silicates as a bond phase. The silicon nitride, which can be formed 'in-situ', is much more refractory than silicate bonds. It does not melt up to its dissociation point of 2200K; thus it would be expected to, and in fact does, retain useful strength to much higher temperatures than silicate bonds.

Washburn and Love[3] have reported properties of a silicon carbide refractory with a complex nitride bond. The bond phase is a combination of various nitrides of silicon with the major nitride present being silicon oxynitride. They report that the

mechanical breakdown characteristics of the nitride and oxynitride are different. The nitride-bonded product resists a high initial impact on crushing, but once broken, it crushes easily. The product with an oxynitride bond, however, has a lower impact resistance, but in crushing further, it is more difficult to break down than the silicon nitride-bonded material. Guzman, et al[6], in a comparative study of nitride and oxynitride-bonded bodies, found the properties quite comparable with the nitride-bonded body slightly better in high temperature deformation behavior.

Washburn[7] compared the oxidation resistance of silicon oxynitride and silicon nitride at several temperatures in air. He found that although both materials showed about the same weight gain, there was considerably more change in the chemistry of the silicon nitride specimen, reflected primarily in the formation of oxynitride and silica. Zabruskova, et al[8] examined the high temperature stability of silicon oxynitride. They report that silicon oxynitride is stable up to 1600K in an inert atmosphere, and that above this temperature it is volatilized, especially at temperatures above 1825K. In oxidizing atmospheres they found its stability is determined by the nature and degree of reaction between the silicon oxynitride and the components of the gaseous atmosphere, and the

nature of any resulting new compounds. They also report that silicon oxynitride reacts vigorously in the gaseous atmosphere created by a silicon carbide furnace at 2050K and above resulting in the formation of cristobalite and silicon nitride.

Kappmeyer, Hubble, and Powers[2] tested many available bonded silicon carbide refractories with respect to those properties most desirable in steel plant environments. They found that, on the average, the nitride - and oxynitride - bonded bodies had higher hot strengths and better abrasion resistance, although there were some oxide-bonded bodies with equivalent properties. In slag tests the nitride - and oxynitride - bonded silicon carbide refractories were superior.

The next major advance in silicon carbide processing occurred in the form of direct or self-bonding. The oldest method of self-bonding, recrystallization at high temperatures, is discussed by Billington, et al[9]. Pellets and test bars of alpha silicon carbide were pressed at 70 MPa and then fired in nitrogen at between 2200 and 3000K. Densities of about 2.6 g/cm^3, near 80% theoretical, resulted with little or no shrinkage observed at firing temperatures below 2800K. Those observations led to the conclusion that the sintering of silicon carbide proceeds by either surface

diffusion or vapor phase transport.

Hot pressing with additives is discussed by Alliegro, et al[10], who discovered that densities greater than 3.0 g/cm^3 can be achieved by hot pressing either the beta or alpha forms with the addition of 1% by weight of aluminum and iron. Pressures as low as 40 MPa with temperatures around 2300K can be used. Other elements have been examined as potential hot pressing aides, but Alliegro observed that iron and aluminum cause the greatest densification, i.e. to greater than 98% of theoretical density. These dense silicon carbides are found to exhibit excellent hot strengths, approaching 700 MPa at 1800K.

Thermal Diffusivity

Thermal diffusivity is the property of a material which determines the transient heat flow through the material and is expressed in m^2/sec. The thermal diffusivity (α) is related to the thermal conductivity (k), density (ρ), and heat capacity (Cp) by the equation:

$$\alpha = \frac{k}{Cp.\rho} \qquad (1)$$

The flash method of measuring the thermal diffusivity was first introduced by Parker, et al[11] in 1961. This method involves introducing a short pulse of radiant energy onto the front face of a thin, disc-shaped sample with parallel faces and then recording

the temperature transient of the rear face. From this record, the thermal diffusivity can be calculated. Parker, et al, showed that the temperature rise of the back face of the sample is described by the equation:

$$V = 1 + 2 \sum_{n=1}^{\infty} (-1)^n \exp(-n^2 \omega), \qquad (2)$$

where $V = T/T_{max}$ is a reduced temperature, $\omega = \pi^2 \alpha t / L^2$, α = thermal diffusivity, t = time, and L = thickness of the sample. Parker arbitrarily chose to use the point where V = 0.5 to calculate ω. When V = 0.5, then $\omega = 1.38$, and the thermal diffusivity is given by:

$$\alpha = 1.38 L^2 / \pi^2 \cdot t_{\frac{1}{2}}, \qquad (3)$$

where $t_{\frac{1}{2}}$ = time to reach one-half the maximum temperature rise of the rear surface of the sample.

The key to the success of using this simple technique for determining the thermal diffusivity from the thermal history of the rear face of the sample lies in fulfilling the assumptions applied to the solution of the heat flow equation. The assumptions which are most difficult to realize are as follows:

(i) The duration of the energy pulse must be very short compared to the thermal diffusion time;

(ii) Heat losses from the sample must be negligible: and

(iii) Heat flow must be one-dimensional.

The first assumption is easily violated, but Taylor

and Cape[12] report that equation (3) is accurate to better than 1% for $\tau/t_c \cdot 0.02$ where τ is the pulse width and $t_c = L^2/\pi^2 \cdot a$. The thickness of samples can generally be adjusted so that this inequality is satisfied.

Assumption (ii) has not been thoroughly discussed in the literature and the effects of departure from it are difficult to evaluate. By making measurements at reduced pressures, heat losses by convection can be reduced. Heat losses by radiation are not significant at low temperatures, but may become important at elevated temperatures. Corrections for radiative heat losses can be made by the method described by Cowan[13]. Heat losses by conduction cause more problems. Since the sample must be in contact with the support system, the sample support can act as a heat sink. When heat loss by conduction occurs through sample supports on the sides of the sample, radial flow can occur, violating assumption (iii).

Branscomb and Hunter[14] discuss ways of minimizing conductive heat losses. They state that these losses can be reduced by supporting the sample on a small area, as well as allowing only very light contact (high thermal resistance) between the circumference of the sample and the support system. When these conditions are met the conductive heat losses and radial heat flow should be negligible due to the short times involved in performing a measurement.

Whether these assumptions have been satisfied can be qualitatively verified by comparing the experimental record of the rear face temperature transient of the sample with a plot of V vs. ω from equation (3) as given by Parker, et al[11].

Kerrisk[15a,b] studied the treatment of heterogenous materials as homogenous for the purposes of thermal diffusivity measurements. He considers the problem theoretically from the viewpoint of the thermal wavelength of the temperature pulse and develops a criterion for determining the minimum sample thickness to satisfy the requirement of homogeneity.

The inequality he derives is:

$$d(f)^{-1/3} < l/M, \quad (4)$$

where d= representative particle diameter, f= volume fraction of the particulate phase, l= sample thickness, and M is an adjustable parameter. Kerrisk claims $100<M<1000$ as reasonable. A value of 100 for M, with f=0.1, and l=4mm lead to an upper limit for particle size of 19μm.

Lee and Taylor[16] in a later experimental study of the thermal diffusivity of dispersed composites found Kerrisk's homogeneity criterion to be overly restrictive. They obtained experimental values for the thermal diffusivity of copper spheres in a solder matrix with volume fractions from 0.01 to 0.3, sample

thickness of 3 to 6 mm, and particle sizes of 400 to 1200μm. These values agreed with calculated values to within 5%. These results show that Kerrisk's assumptions as to reasonable values for M need further study, especially in a wider range of materials, such as ceramics.

III. Experimental Procedures

Material

The material investigated in this study is a commercial product[a]. It is stated to be a silicon carbide refractory with silicon oxynitride as the major component of the bond phase. Table I gives a typical chemical analysis of the refractory. The samples examined after service were used as the inner wall of a vertical zinc retort at the New Jersey Zinc Company's Palmerton, Pa. plant for three years of continuous service. Specimens were taken from the inside surface (that surface which was exposed to the zinc ore/coke charge), this surface is subjected to continuous erosive wear by the charge so that new material is continuously being exposed, the middle portion of the wall, and the outside surface (that exposed to the heating space), as well as in the 'as-received' condition. The 'as-received' samples are designated NA, the samples subjected to three years service will be designated NG, followed by an "I" for the inside surface samples, an "M" for the middle portion samples, and an "O" for samples from the outside surface.

Characterization

1. X-ray Diffraction

   Standard x-ray powder diffractometry techniques and equipment were utilized to identify the

[a] CN-163, The Norton Company, Worchester, Ma. 01606

TABLE I

Chemical Composition and Properties

of 'As-received' Samples*

Typical Chemical Analysis (% by weight):

Silicon	67.3
Carbon	26.7
Nitrogen	3.6
Oxygen	1.4
Other metals	1.0

Bulk Density (g/cm^3):	2.60
Apparent Porosity (%):	15
Thermal Conductivity (W/m·K):	9.61

*Norton Product Information S-P-C-BD3, July 1974.

crystalline phases present in each sample.

The samples were crushed to-325 mesh and screened onto a glass slide. The slides were than mounted in a Siemen's diffractometer[b]. The difractometer was operated at a scan speed of 1° 2θ per minute using nickel filtered, Cu K_α radiation.

2. Thermal Expansion

Linear thermal expansion curves were obtained for each sample over the temperature range from room temperature to 1400K using an automatic recording dilatometer[c]. Samples were in the form of rectangular bars measuring 5.08 ± 0.05 cm long. These samples were heated at the rate of 3K per minute then allowed to furnace cool. To prevent oxidation of the brick to form a glassy phase, the expansion measurements were made with sample contained in an argon ambient. Percent linear expansion was plotted versus temperature and mean thermal expansion coefficients were calculated by dividing the percent expansion by the change in temperature.

3. Scanning Electron Microscopy

Representative samples were fractured and the fracture surfaces were coated with carbon. The samples were observed using an ETEC scanning electron microscope[d] at several magnifications.

[b] Chrystalloflex IV, Siemen's America, Inc., New York, N. Y. 10001

[c] Orton Automatic Recording Dilatometer, The Edward Orton, Jr. Ceramic Foundation, Columbus, Oh. 43201

[d] Autoscan U-1, FTEC Corp., Hayward, Ca. 94545

4. Optical Microscopy and Grain Size Distribution Analysis

Samples were vacuum impregnated with epoxy, rough ground on a diamond grinding wheel, then polished using diamond paste with grit sizes of 15, 6 and 1μm. The polished samples were examined using a reflected light microscope[e].

Grain size distribution analysis was performed using an image analyzer[f] attached to the microscope and interfaced to a programable calculator[g] which did the on-line statistical analysis.

Thermal Diffusivity versus Temperature

Thermal diffusivities were measured by the laser-flash technique. Discs, 0.3 cm thick and 1.27 cm in diameter, were held in a graphite specimen holder in a vertical tube, graphite resistance, nitrogen atmosphere furnace[h]. Thermal diffusivity was measured using a 1.06μm Nd-glass rod laser[i] as the transient heat source, and monitoring the temperature response of the rear face by means of an IR detector[j] connected through a bias circuit to an oscilloscope[k] equipped with signal storage. The sensitivity of the IR detector was such that measurements could be obtained only at specimen

[e] Axiomal, Carl Zeiss, Inc., New York, N. Y. 10018
[f] IIMC, Millipore Corp., Bedford, Ma. 01730
[g] 600-14, Wang Laboratories, Inc., Tewksbury, Ma. 01876
[h] 1000A, Astro Industries, Santa Barbara, Ca. 93101
[i] K-1, Korad Co., Santa Monica, Ca. 90406
[j] IT-7, Barnes Engineering Co., Stamford, Co. 06902
[k] 1201A, Hewlett-Packard, Palo Alto, Ca. 94304

temperatures above 600K. Since the service temperature for the bricks is 1700K, measurements were made up to this temperature. The ambient temperature of the specimen was changed by adjusting the temperature of the carbon resistance furnace. Further details of the apparatus are given in Appendix A and B.

IV. Results

Characterization

1. X-ray Diffraction

The results of the powder diffraction analysis are given in Table II. These results show that the matrix of NA is composed of a mixture of α-and β-Si_3N_4 with some Si_2N_2O present. In all three NG samples the matrix appears to be primarily composed of Si_2N_2O with some α-and β-Si_3N_4. The silicon carbide is an alpha polytype designated 6H.

2. Thermal Expansion

Figures 1 through 4 show the thermal expansion curves measured for each of the samples; the calculated mean linear thermal expansion coefficients are given in Table III. The coefficients of the NG samples are 10 to 15% lower than the coefficient of the NA sample.

3. Scanning Electron Microscopy

Scanning electron photomicrographs of fracture surfaces of the four samples are shown in Figures 5 through 12. Figures 5 and 6 show the multiphase nature of the bonding matrix in sample NA. The large smooth features can be identified as silicon carbide grains due to their size and metallic appearance to the naked eye. The needle-like particles can be identified as Si_3N_4 as discussed by Forgeng and

TABLE II

X-ray Diffraction Results

d(nm)	Relative Intensities ($\%I/I_o$)							
	NA	NG-I	NG-M	NG-O	α-SiC	α-Si_3N_4	β-Si_3N_4	Si_2N_2O
	Observed Intensities				JCPDS Standard Intensities			
.468	4	13	39	37				80
.444	5	18	79	61				100
.336	6	28	99	85				100
.331	2	3	8	5			85	
.274		5	16	12				30
.267	9	6	22	9			100	
.262	20	16	82	41	40			
.260		10	36	24		75		50
.255	28	10		19		100		
.251	100	100	100	100	100		100	
.242		9	31	22				80
.238		10	31	20				80
.235	29	29	54	29	20			
.229			20	9				50
.217	12	11	25	10	10		35	50
.168	3	5	10	7				50
.160	3	4	14	9		35	20	50
.154	17	21	61	31	35			
.147		5	7	5				50
.142	4	7	25	9	15			
.131	19	15	43	20	40		17	50
.129	2	4	10	9	15		85	
.126	4	3	16	7	7		85	50

α-SiC - JCPDS(22-1273), α-Si_3N_4 - JCPDS(9-250)

β-Si_3N_4 - JCPDS(9-259), Si_2N_2O - JCPDS(18-1171)

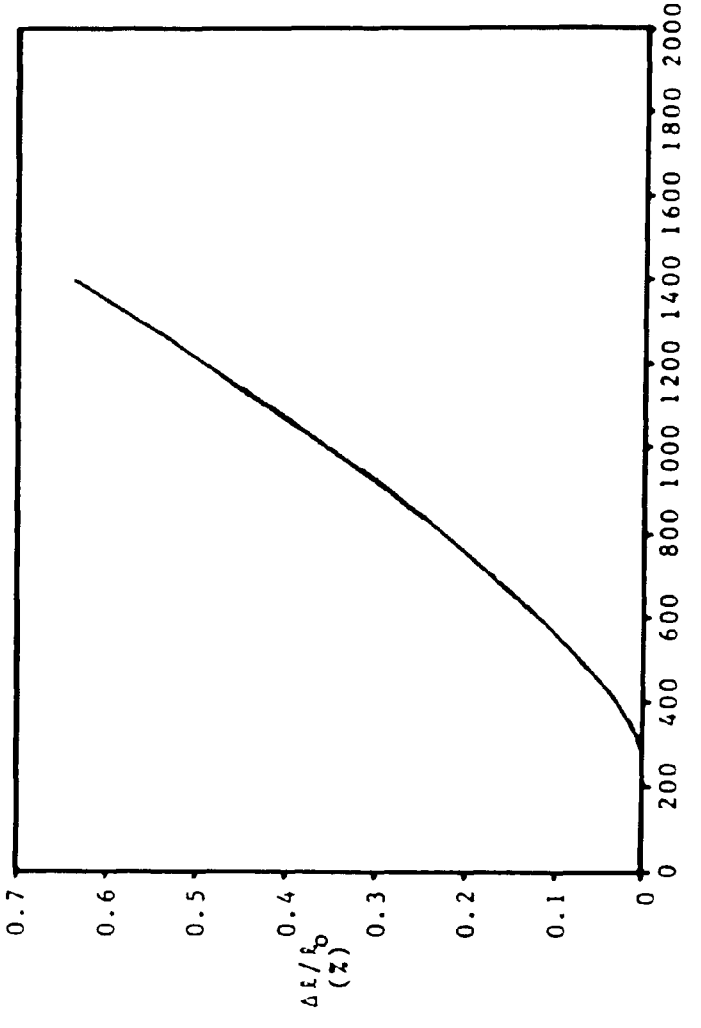

FIGURE 1. Thermal Expansion of Sample NA.

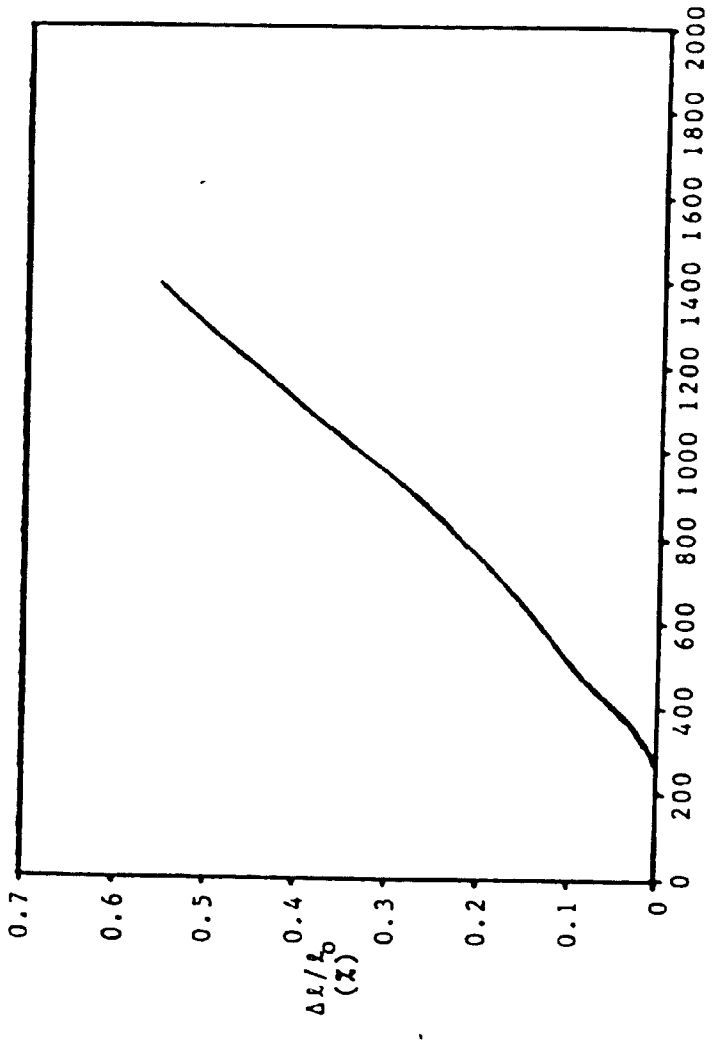

FIGURE 2. Thermal Expansion of Sample NG-1.

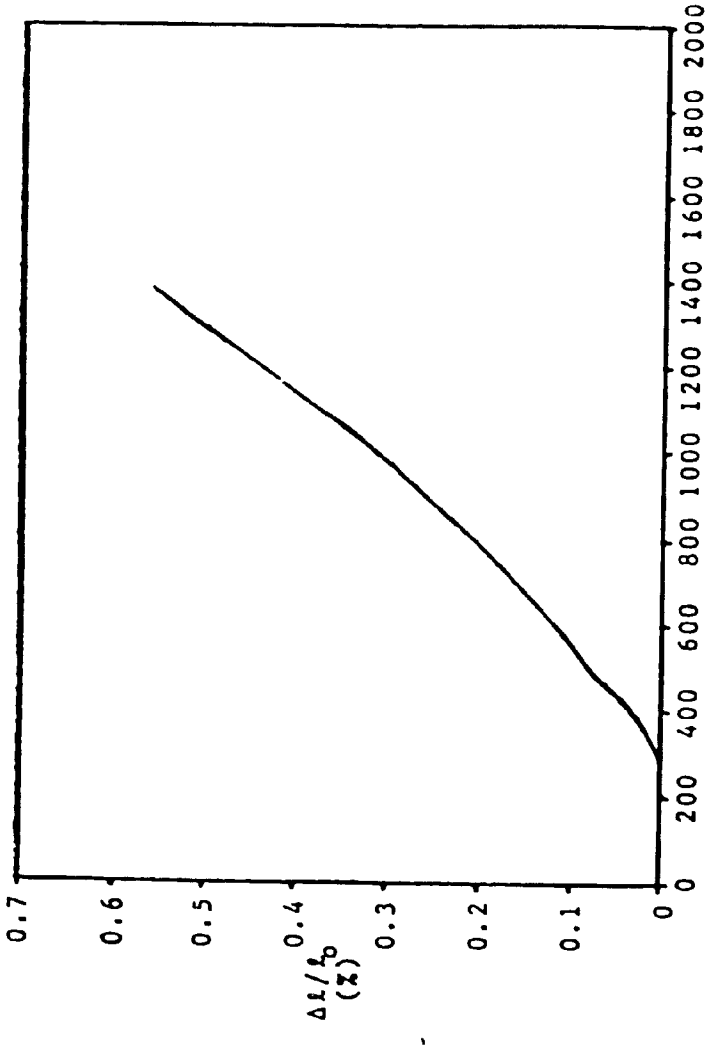

FIGURE 3. Thermal Expansion of Sample NC-M.

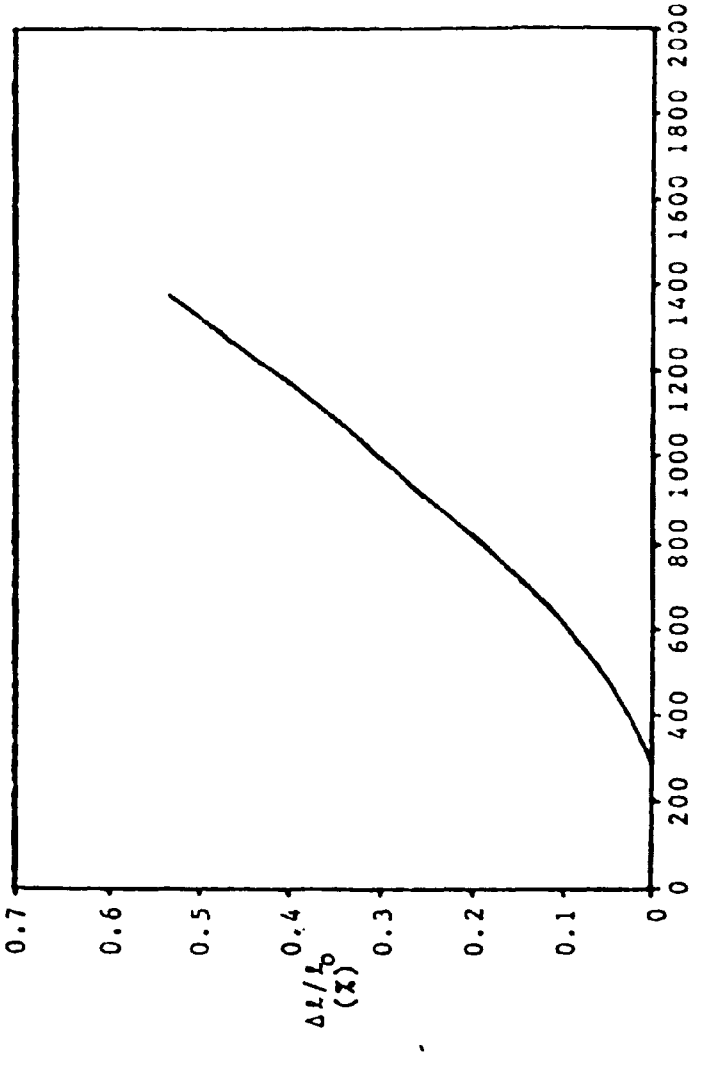

FIGURE 4. Thermal Expansion of Sample MG-0.

TABLE III

Calculated Mean Linear Thermal Expansion Coefficients

(300K to 1400K)

NA	NG-I	NG-M	NG-O
5.82×10^{-6}/K	5.14×10^{-6}/K	5.14×10^{-6}/K	5.14×10^{-6}/K

TABLE IV

Calculated Average Grain Sizes

	NA	NG-I	NG-M	NG-O
Average Grain Size (μm)	41.6	42.9	41.0	38.7
Standard Deviation	36.9	37.8	37.0	35.7

FIGURE 5. Scanning Electron Photomicrograph of Sample NA. Magnification 800X.

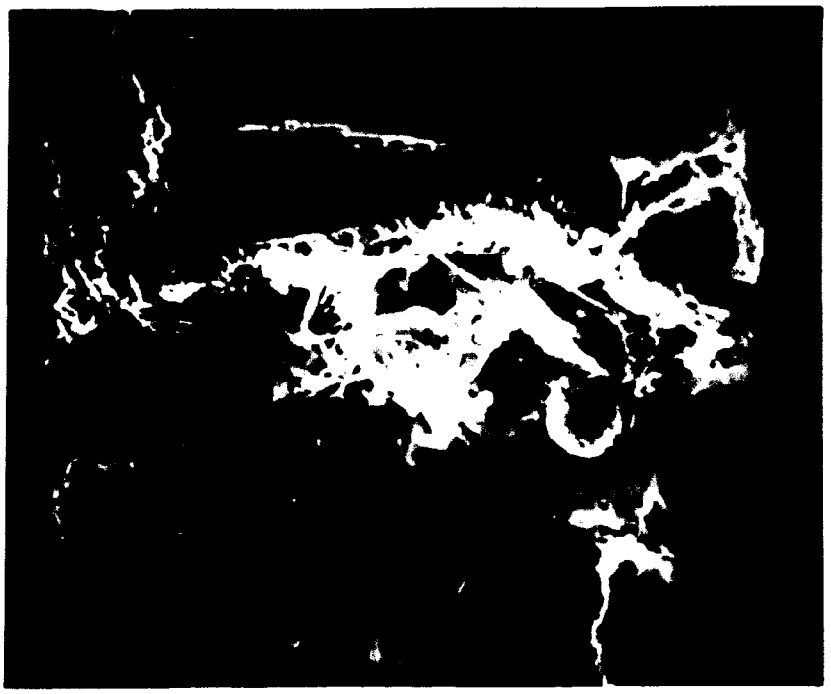

FIGURE 6. Scanning Electron Photomicrograph of Sample NA. Magnification 1900X.

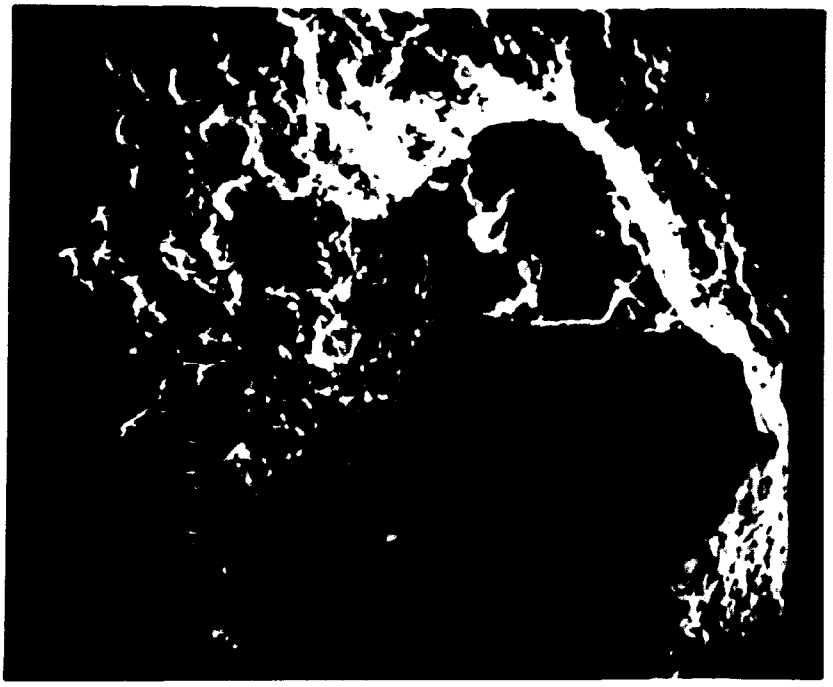

FIGURE 7. Scanning Electron Photomicrograph of Sample NG-I. Magnification 720X.

FIGURE 8. Scanning Electron Photomicrograph of Sample NG-I. Magnification 3400X.

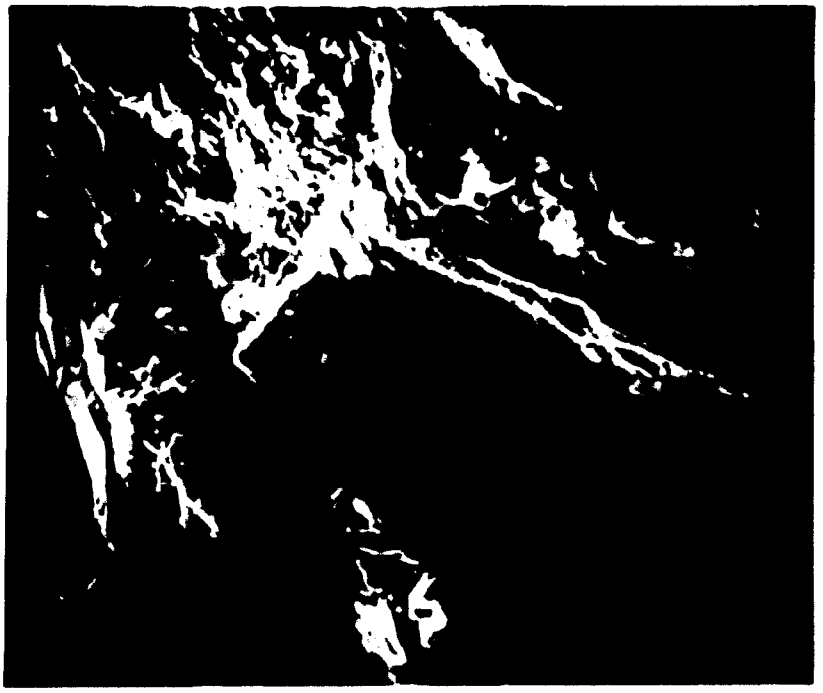

FIGURE 9. Scanning Electron Photomicrograph of NG-M. Magnification 800X.

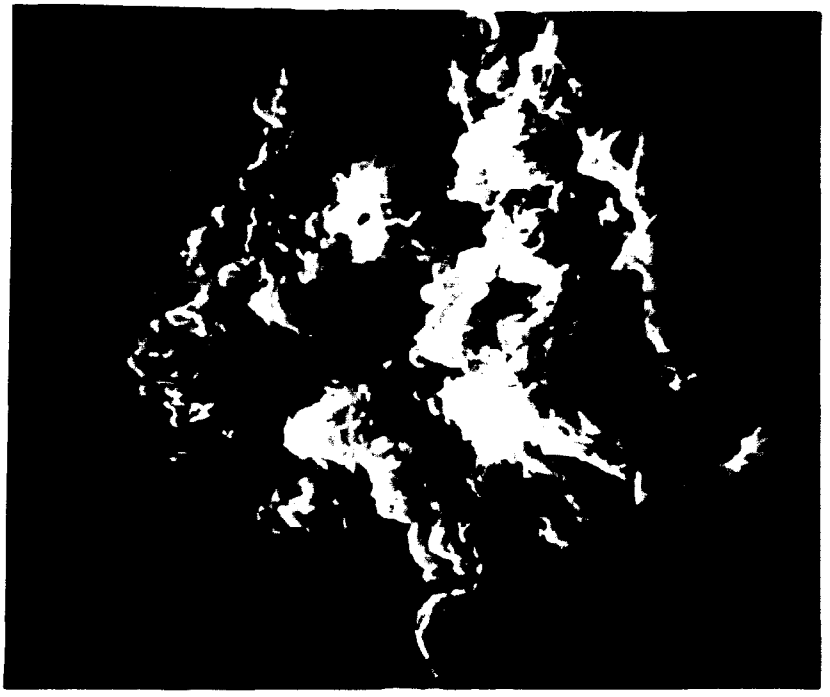

FIGURE 10. Scanning Electron Photomicrograph of Sample NG-M. Magnification 4000X.

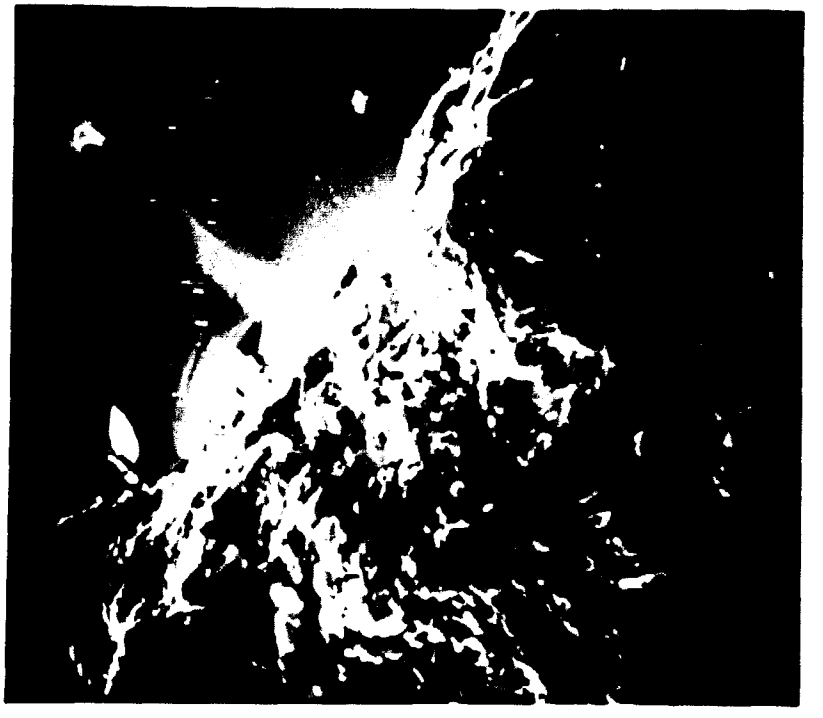

FIGURE 11. Scanning Electron Photomicrograph of Sample NG-0. Magnification 800X.

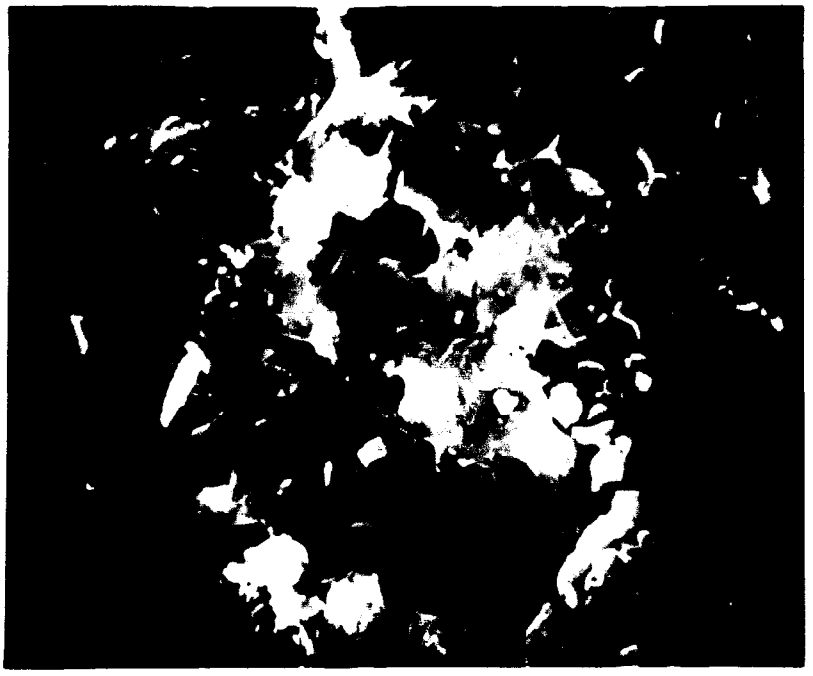

FIGURE 12. Scanning Electron Photomicrograph of Sample NG-0. Magnification 4000X.

Decker[17] and Jones, Pitman and Lindley[18]. The smoother, more granular phase is Si_2N_2O. The matrix of the NG samples, Figures 7 through 12, appears to be single phase as can be seen by the absence of needle-like particles.

4. Optical Microscopy and Grain Size Distribution Analysis

Figures 13 through 16 are optical photomicrographs of polished sections of the four samples. The light gray features are silicon carbide grains. The darker mottled gray areas are pores and the darkest areas are the bonding matrix. The amount of pore area visible in sample NA is much greater than in any of the NG samples. The wide range of grain sizes apparent in these micrographs is confirmed by Figures 17 through 20 which show the results of silicon carbide grain size distribution analysis. The calculated average grain sizes and standard deviations are given in Table IV. The grain size distributions are all quite comparable. The average grain size of sample NG-I is slightly higher than that of sample NA. Sample NG-M has approximately the same average grain size than sample NA. Sample NG-O has a lower average grain size than Sample NA. Some unreacted silicon was observed in the 'as-received' sample.

FIGURE 13. Optical Photomicrograph of Sample NA. Magnification 50X.

FIGURE 14. Optical Photomicrograph of Sample NG-I. Magnification 50X.

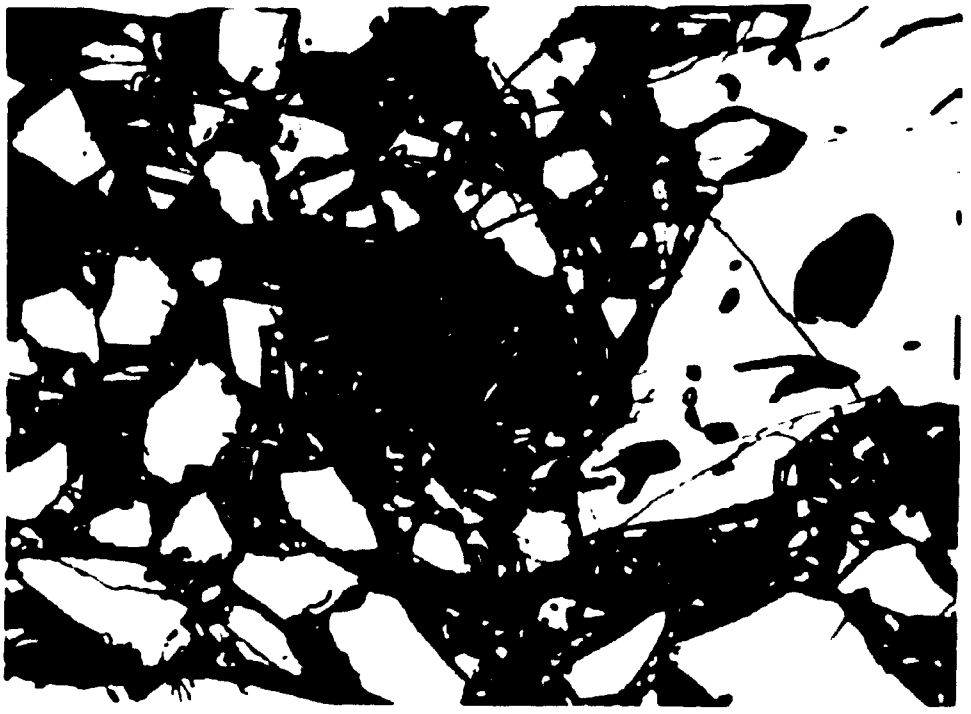

FIGURE 15. Optical Photomicrograph of Sample NG-M. Magnification 50X.

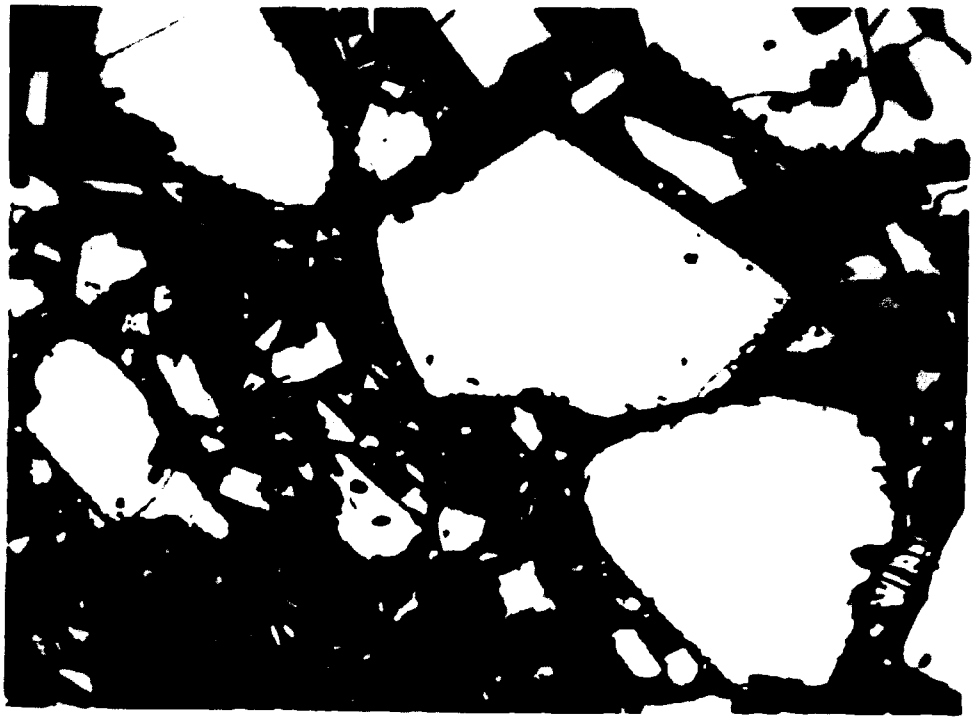

FIGURE 16. Optical Photomicrograph of Sample NG-0. Magnification 50X.

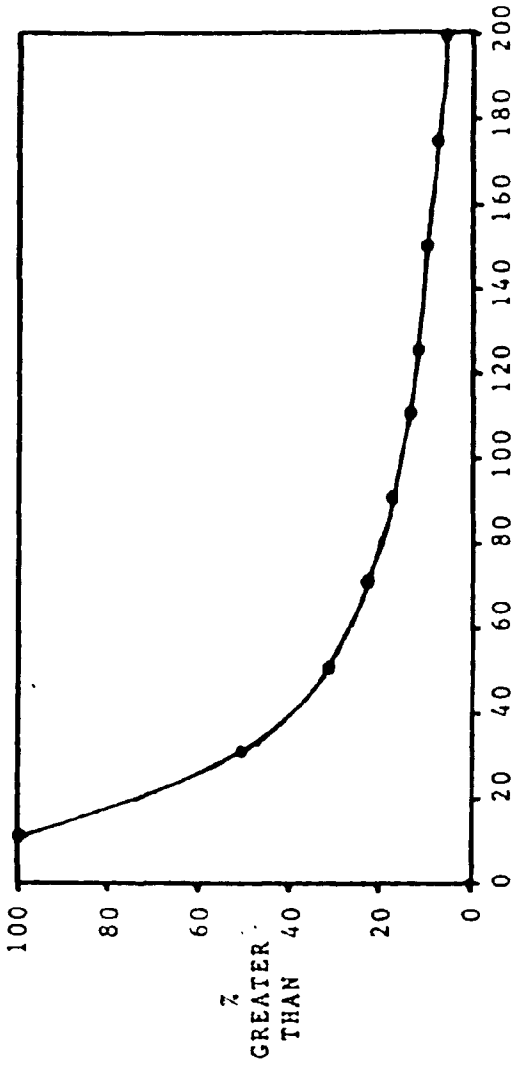

FIGURE 17. Grain Size Distribution of Sample NA.

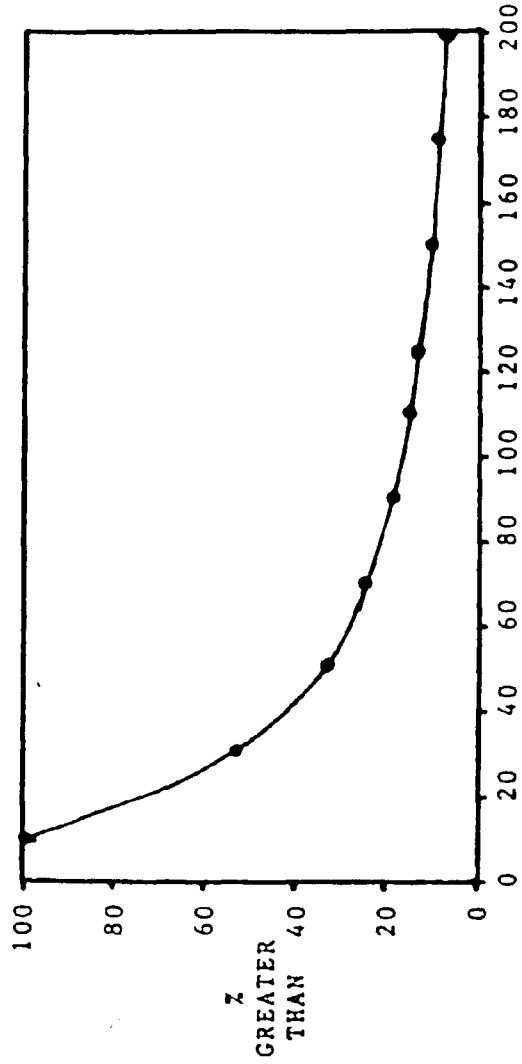

FIGURE 18. Grain Size Distribution of Sample NG-1.

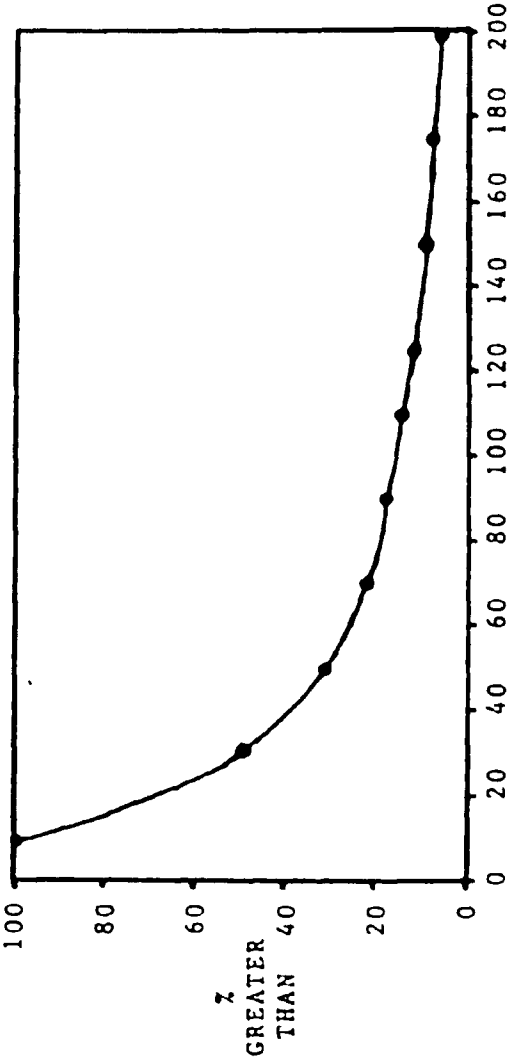

FIGURE 19. Grain Size Distribution of Sample NG-M.

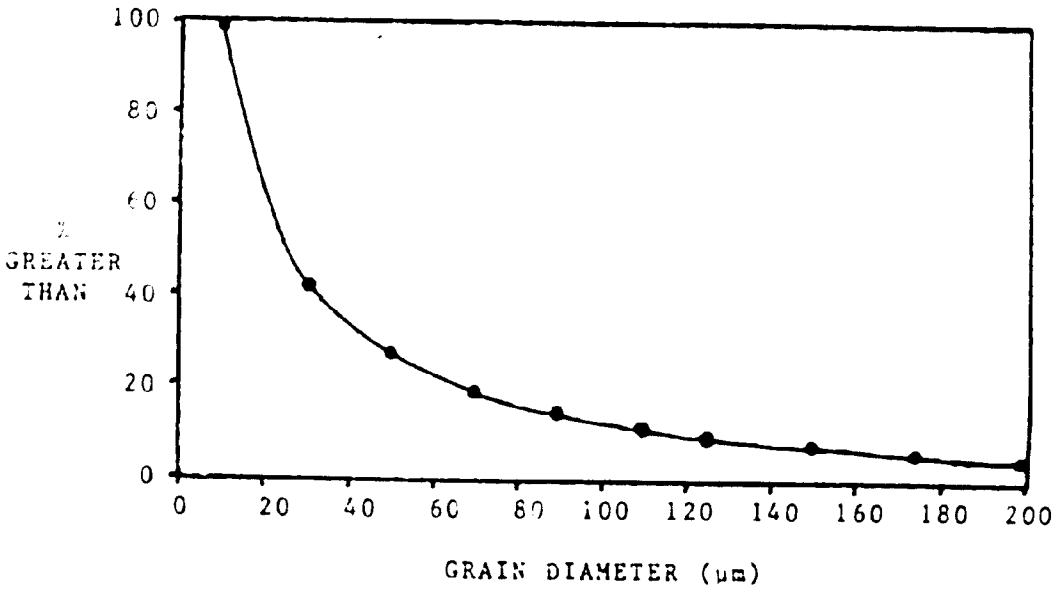

FIGURE 20. Grain Size Distribution of Sample NG-0.

Thermal Diffusivity versus Temperature

The thermal diffusivities of all four samples, Figures 21 through 24, show a decrease of approximately 50% on heating from 600 to 1700K. The NA sample has a thermal diffusivity approximately 20 to 30% lower than the NG samples across the entire temperature range. The exception to this is a sample taken from the immediate outside surface which has a thermal diffusivity comparable to NA. (Curve B in Figure 24).

Using Kerrisk's[4a,b] homogeneity criterion, equation (4), with d as the average grain size, approximately 40 μm, f as 0.8, the assumed volume fraction of the silicon carbide grains, and l as 0.3 cm, the sample thickness leads to a value of 70 or less for M in order to satisfy the inequality of equation (4). Thermal diffusivity values calculated using equation (1) and properties listed in Table I yield results which compare within 10% of measured values at 1300K.

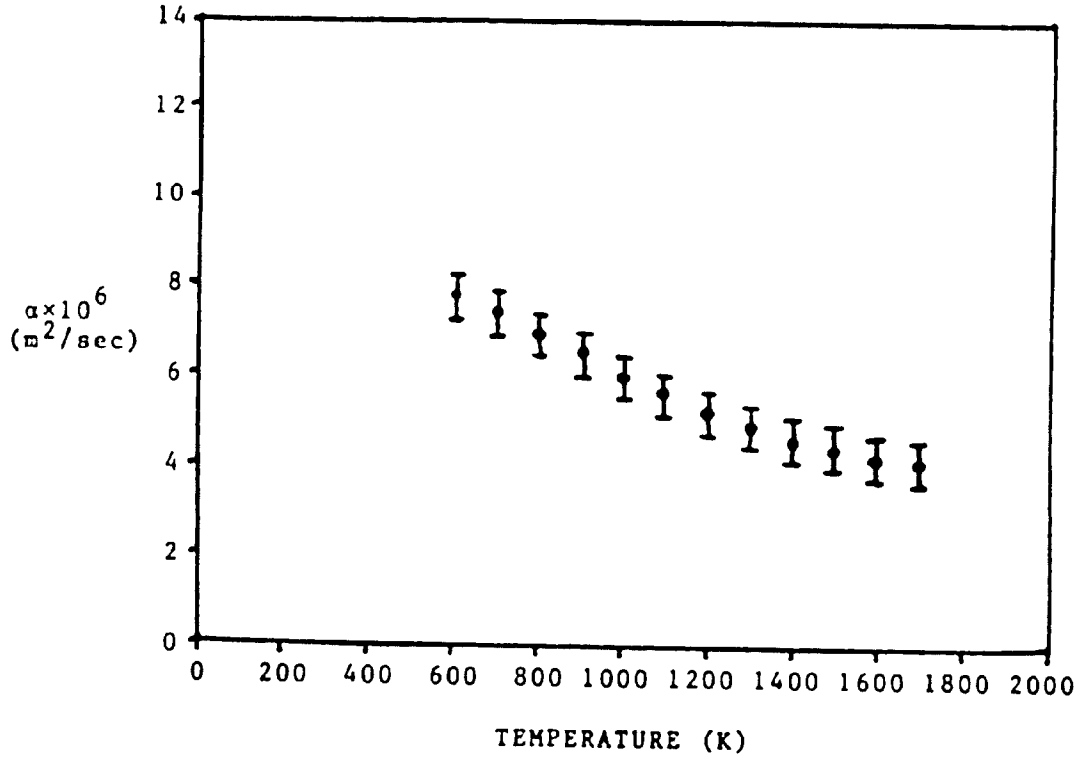

FIGURE 21. Variation of Thermal Diffusivity with Temperature for Sample NA.

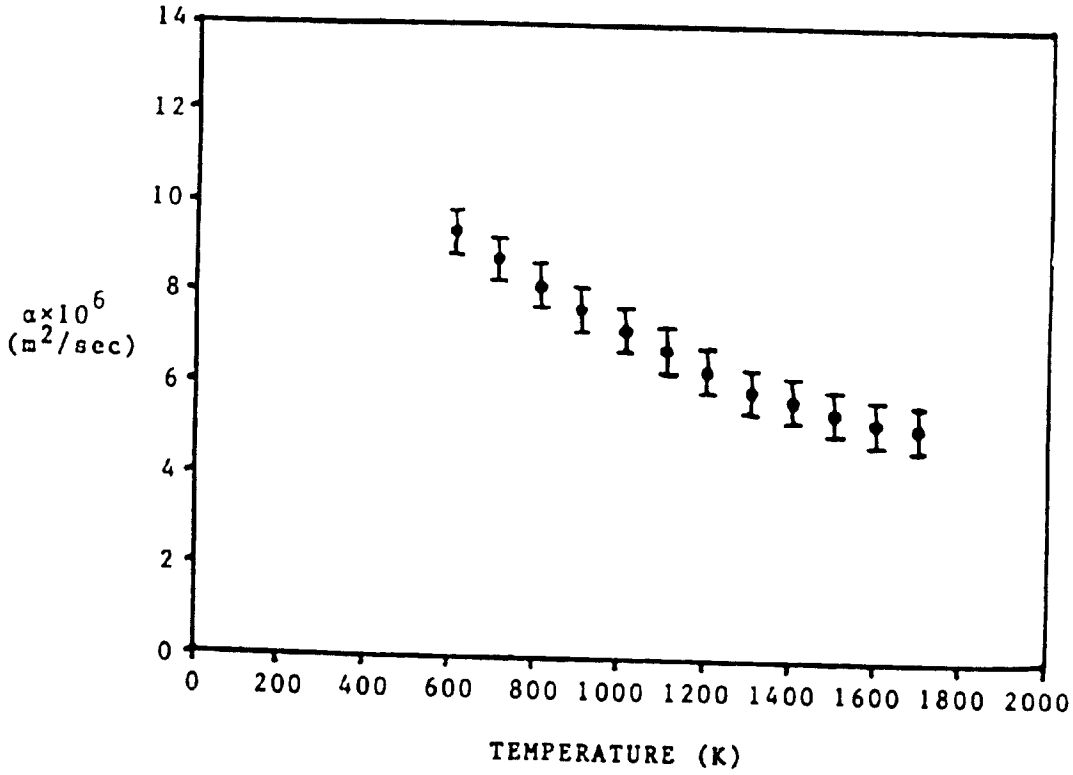

FIGURE 22. Variation of Thermal Diffusivity with Temperature for Sample NG-I.

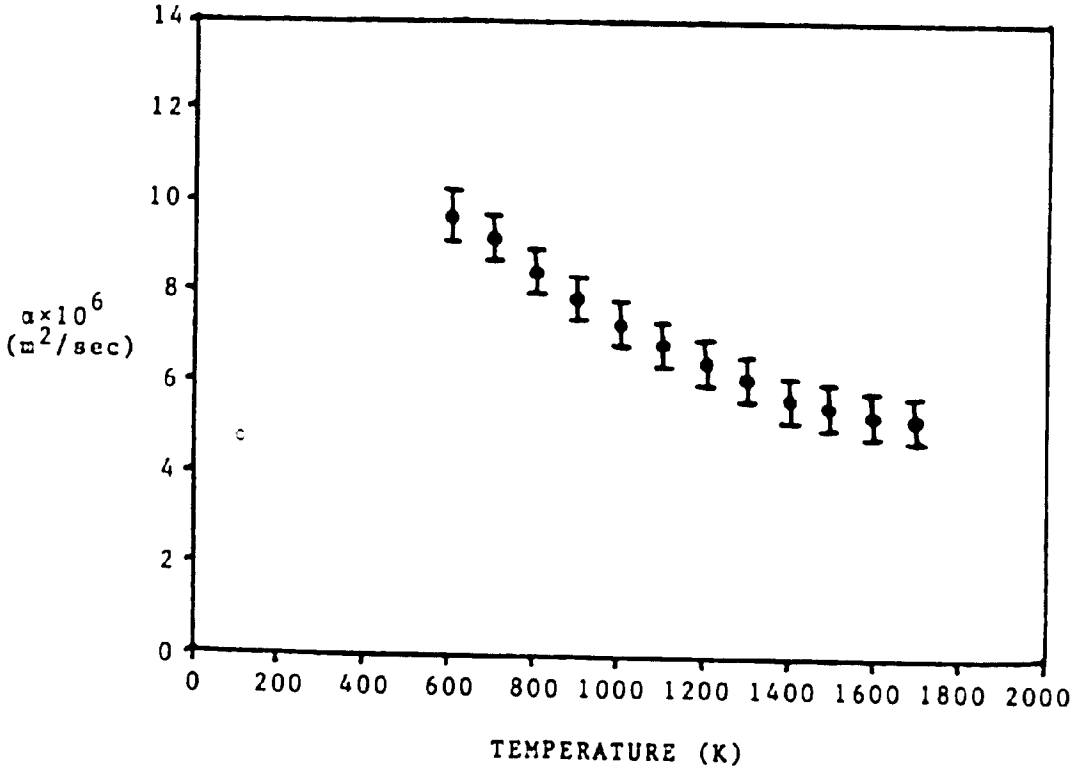

FIGURE 23. Variation of Thermal Diffusivity with Temperature for Sample NG-M.

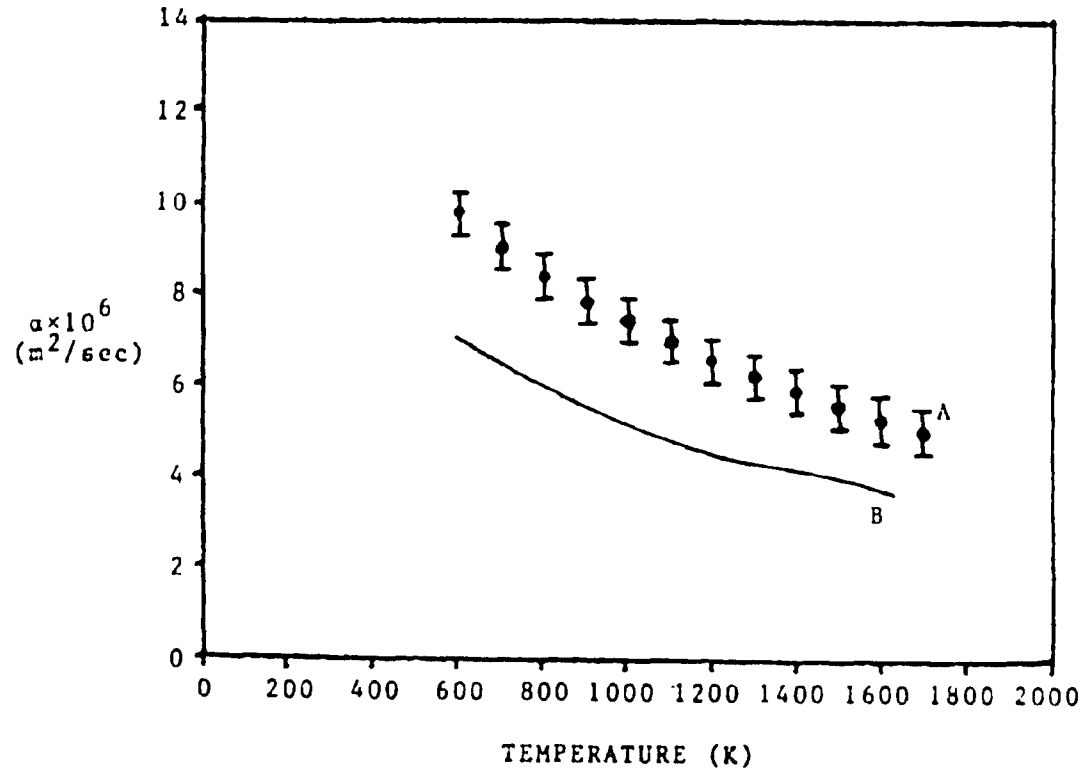

FIGURE 24. Variation of Thermal Diffusivity with Temperature for Sample NG-0. Curve A gives the results for a sample taken from slightly beneath the outside surface of the brick. Curve B shows the results for a sample taken from the immediate outside surface of the brick, with the glassy slag removed.

V. Discussion

The bonding matrix of the 'as-received' brick is a multi-phase mixture of α- and β-Si_3N_4 with Si_2N_2O. This is confirmed by the x-ray powder diffraction analysis and scanning electron photomicrographs. The scanning electron photomicrographs seem to indicate a larger amount of Si_2N_2O in the NA sample than the x-ray data would suggest. This could indicate that the Si_2N_2O is poorly crystallized in the 'as-received' brick. Both the x-ray results and the scanning electron photomicrographs confirm that the NG samples have a predominantly single phase matrix composed of Si_2N_2O.

The stability of the silicon carbide grain in the severe environment of the zinc retort is shown by the small changes in grain size distribution. The slight increase in the average grain size of the inside surface sample, NG-I, as compared to the NA sample could result from the corrosion and erosion to which the inside surface of the bricks is subjected by the moving zinc ore/coke briquets. This corrosion and erosion results in a decrease in wall thickness of approximately 2.5 cm in three years of service. There is no observed zinc penetration of the brick. This would indicate an erosive type of action occurring at the inside surface of the brick. The smaller sized grains

would be pulled out or worn away at a more rapid rate than the large grains. This would result in an increase in the average grain size as was observed. The negligible amount of change in the average grain size and distribution of grain sizes of the middle portion sample, NG-M, as compared to the NA sample shows the excellent high temperature stability of the silicon carbide grains. The decrease in the average grain size and change in the grain distribution of the outside surface sample, NG-O, as compared to the NA sample is difficult to explain. It could be a consequence of fragmentation of some of the grains due to thermal shock effects on retort shutdown or evidence of attack on the grains by a glass-like slag which coats the outside surface of these bricks after three years service. Figure 25 shows this slag coating which can be seen to penetrate the brick itself. Neither hypothesis can be unequivocally confirmed on the basis of available data.

The increase in thermal diffusivity observed in the NG samples could be the result of improved crystallinity of the Si_2N_2O portion of the bonding matrix as well as the decrease in apparent porosity evidenced by the optical photomicrographs. This decrease in porosity may be the result of compression of the bricks due

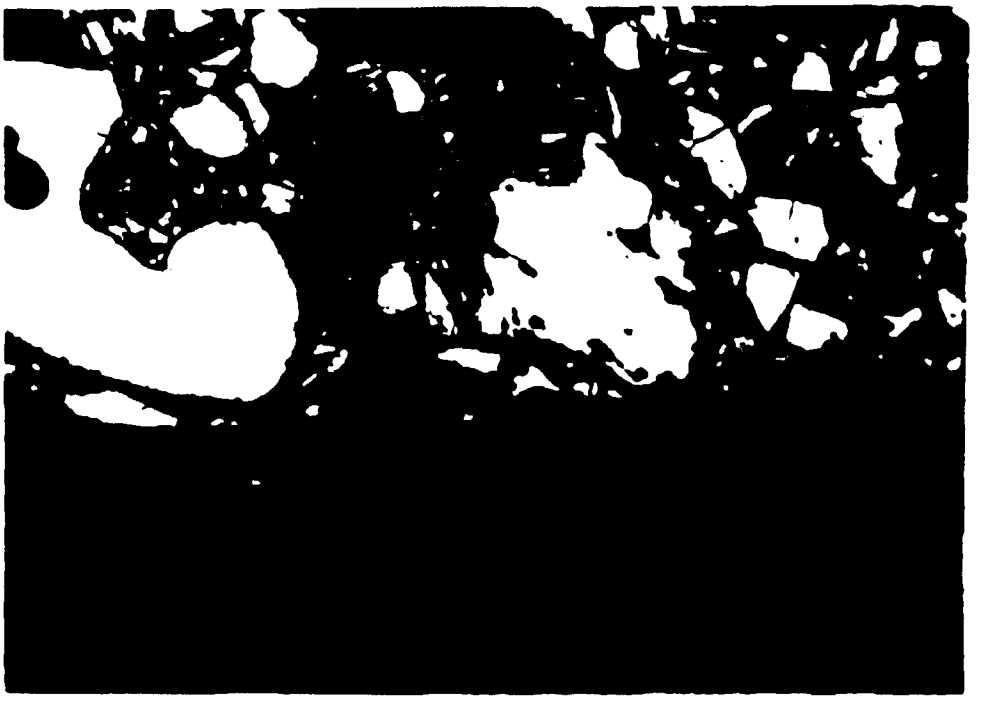

FIGURE 25. Optical Photomicrograph of Outer Surface of Refractory. Micrograph shows the glassy slag which coats the outer surface of brick as can be seen also penetrates the brick itself. Magnification 50X. Glassy slag is in lower portion of micrograph.

to the restraint imposed on the thermal expansion of the wall by the end walls of the retort. The lower thermal diffusivity of the immediate outside face sample can be explained in terms of the penetration of the glass-like slag as shown in Figure 25.

The decrease in the thermal expansion coefficient exhibited by the NG samples probably is also the result of the higher degree of crystallinity of the Si_2N_2O portion of the bonding matrix of the brick.

VI. Summary and Conclusions

The bonding matrix of this brick changes from an initially multi-phase mixture of silicon nitride and poorly crystallized silicon oxynitride to a predominantly single-phase matrix composed of well crystallized silicon oxynitride. This transformation is thought to occur by oxidation of the silicon nitride to form silicon oxynitride and silicon monoxide (as observed by Guzman, et al[6]) and the further crystallization of the silicon oxynitride already present in the matrix. The silicon monoxide which forms is believed to form the basis of the glassy slag which coats the outside surface of the bricks.

The apparent porosity is a decreased considerably over three years of service. This is believed to be the result of compressive forces developed throughout the entire wall as a result of constrained thermal expansion of the material. The silicon carbide grains are very stable in this environment. Only slight changes in the grain size distribution are observed. The increase in the average grain size of the inside surface sample is believed due to the erosive wear of that surface by the zinc ore/coke charge. The decrease in the average grain size of the outside surface sample is thought to result from thermal shock effects or slag attack.

The decrease in the linear thermal expansion coefficient and increase in the thermal diffusivity are both thought to result from the improved crystallinity of the Si_2N_2O portion of the bonding matrix. The decrease in apparent porosity also contributes to the increase in the thermal diffusivity.

In conclusion a definite correlation was observed between changes in the microstructure and changes in the thermal properties of this bonded silicon carbide refractory body.

REFERENCES

[1]Butler,G.M.,"The Past and Future of Silicon Carbide", J. Electrochem. Soc.,104 (10)640-44 (1957).

[2]Kappmeyer,K.K., Hubble,D.H., and Powers,W.H., "Investigation of Silicon Carbide Brick", Am. Ceram. Soc. Bull., 45 (12)1060-64 (1966).

[3]Washburn,M.E. and Love,R.W., "A Silicon Carbide Refractory with a Complex Nitride Bond Containing Silicon Oxynitride", ibid., 41 (7)447-49 (1962).

[4]Bunce,E.H. and Handwerk,E.C., "New Jersey Zinc Company Vertical Retort Process", Trans. AIME 121, 427-40 (1936).

[5]Shaffer,P.T.B., "A Review of the Structure of Silicon Carbide", Acta Cryst., B25, 477-88 (1969).

[6]Guzman,I.Ya., Tumakova,E.I., and Fedotov,A.V., "Comparative Study of Some Properties of Materials Based on the Compositions SiC-Si_3N_4 and SiC-Si_2ON_2". Ogneupory, (10) 44-48 (1972).

[7]Washburn,M.E., "Silicon Oxynitride Refractories", Am. Ceram. Soc. Bull., 46 (7)667-71 (1967).

[8]Zabruskova,N.T., Guzman,I.Ya., and Dmitriev,I.A., "Stability of Silicon Oxynitride at High Temperatures", Ogneupory, (2)52-55 (1972)

[9]Billington,S.R., Chown,J., and White A.E.S., "The Sintering of Silicon Carbide", in Special Ceramics 1964 ed. P. Popper, Academic Press, New York, 1965. pp 19-27

[10]Alliegro,R.A., Coffin,L.B., and Tinklepaugh,J.R., "Pressure Sintered Silicon Carbide", J. Am. Ceram. Soc. 39 (11)386-89 (1956).

[11]Parker,W.J., Jenkins,R.J., Butler,C.P., and Abbott,G.L., "Flash Method of Determining Thermal Diffusivity, Heat Capacity, and Thermal Conductivity", J. Appl. Phys., 32 (9)1679-84 (1961).

[12]Taylor,R.E. and Cape,J.A., "Finite Pulse-Time Effects in the Flash Diffusivity Technique", Appl. Phys. Lett. 5 (10)212-12 (1964).

[13]Cowan,R.D., "Pulse Method of Measuring Thermal Diffusivity at High Temperatures", J. Appl. Phys., 34 (4,P .1) 926-27 (1963).

[14]Branscomb,T.M. and Hunter,O.,Jr., "Improved Thermal Diffusivity Method Applied to TiB_2,ZrB_2, and HfB_2 from 200°-1300°C", ibid., 42 (6)2309-15 (1971).

[15]a. Kerrisk,J.F., "Thermal Diffusivity of Heterogeneous Materials", ibid., 42 (6)267-71 (1971).
b. Kerrisk,J.F., "Thermal Diffusivity of Heterogeneous Materials. II. Limits of the Steady-State Approximation", ibid., 43 (1)112-17 (1972).

[16]Lee,H.J. and Taylor,R.E., "Thermal Diffusivity of Dispersed Composites", ibid., 47 (1)148-51 (1976).

[17]Forgeng,W.D. and Decker,B.F., "Nitrides of Silicon", Trans. AIME, 212 (6)343-48 (1958).

[18]Jones, B.F., Pitman,K.C. and Lindley,M.W., "The Development of Strength in Reaction Sintered Silicon Nitride", J. Mat. Sci., 12 563-76 (1977).

Appendix A

Experimental Configuration and Allignment

Figure A1 shows a schematic diagram of the apparatus. The system is set up on three levels. A He-Ne alignment laser[a], the Nd-glass pulse laser, and three front surface mirrors are attached to an aluminum plate to form the top level. The infra-red detector and a fourth front surface mirror are attached to an aluminum plate to form the bottom level. The graphite resistance furnace comprises the middle level. The two aluminum plates and the furnace are mounted on the furnace support column and braced by an external support.

The furnace and detector should be isolated as much as possible from mechanical vibrations and strong electric fields. Both of these tend to increase the noise level of the signal as observed on the oscilloscope making measurements more uncertain. An example of the appearance of an experimental trace with sample calculations is given in reference 14, Figure 3.

The system is aligned by initially using the He-Ne laser with no sample in the furnace. Front surface mirrors one and two are adjusted so that the beam from the He-Ne laser travels down the axis of the Nd-glass laser rod. Mirror three is then positioned so that the beam travels down the axis of the furnace. That completes

[a]Edmund Scientific Co., Barrington, N. J. 08007

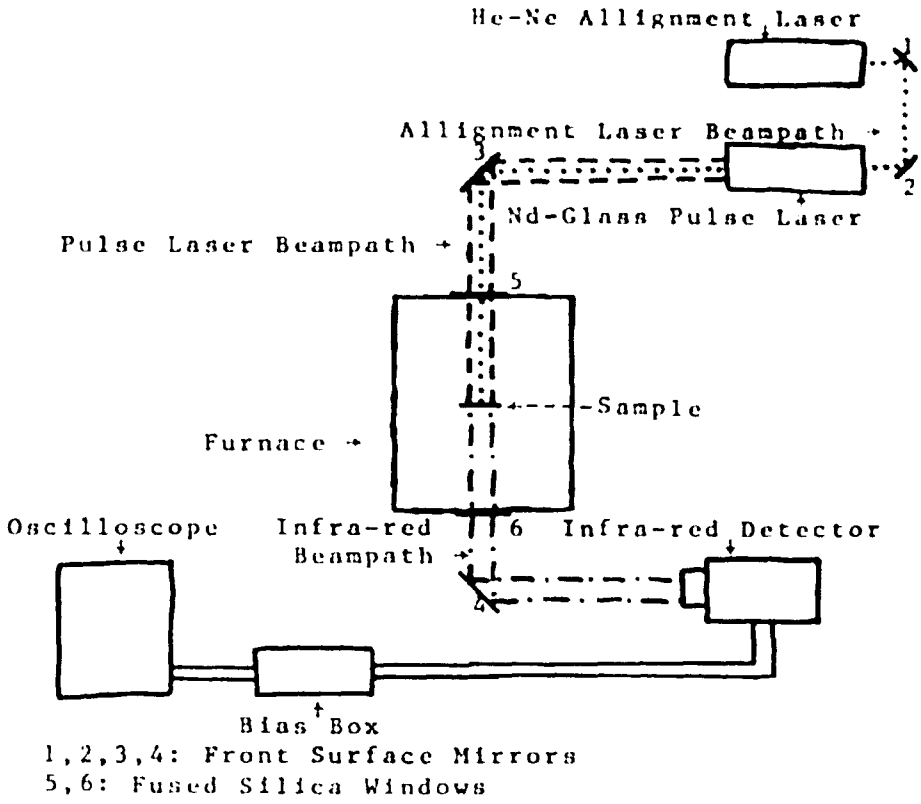

FIGURE A1. Schematic Diagram of Experimental Apparatus.

the rough allignment of the system. Test shots are then fired with the Nd-glass laser using unexposed Polaroid type film in the position of the sample. Final adjustment of mirror three is accomplished by observing the burn pattern produced on the film. A sample is then placed in the furnace and the furnace is raised to a temperature of approximately 1000K so that the sample is visible through the lower fused silica window. Mirror four is then adjusted for peak detector response and the detector is focused on the sample. This completes alignment of the system.

Appendix B

Thermocouple Measurement Technique and System Sensitivity

Due to the spectral sensitivity of the infra-red detector measurements using that method of following the temperature transient on the rear face of the sample is limited to temperatures greater than approximately 600K. An alternate method of following the temperature transient is using a differential thermocouple attached to the back of the sample. To accomplish this a thermocouple port is inserted in place of the lower fused silica window and a Chromel-Alumel differential thermocouple is inserted into the furnace. One bead of the thermocouple is attached to the back of the sample using a silicate-porcelain cement[a]. The thermocouple leads were connected to a millivolt amplifier[b] which in turn was connected to the oscilloscope.

When data obtained using the thermocouple technique was compared with that obtained using the infra-red detector technique a discrepancy was found to exist. Figures B1 and B2 show the results of comparative measurements on two different samples. Figure B1 shows the results for a sample of 1023 steel. Curve 1 was measured using the infra-red detector. Curves 2 and 3 were measured using a differential thermocouple. For Curve 2, the thermocouple was cemented to the back of the sample.

[a]Omega CC High Temperature Cement, Omega Engineering, Inc. Stamford, Ct. 06907

[b]Omni-Amp II, Omega Engineering, Inc., Stamford, Ct. 06907

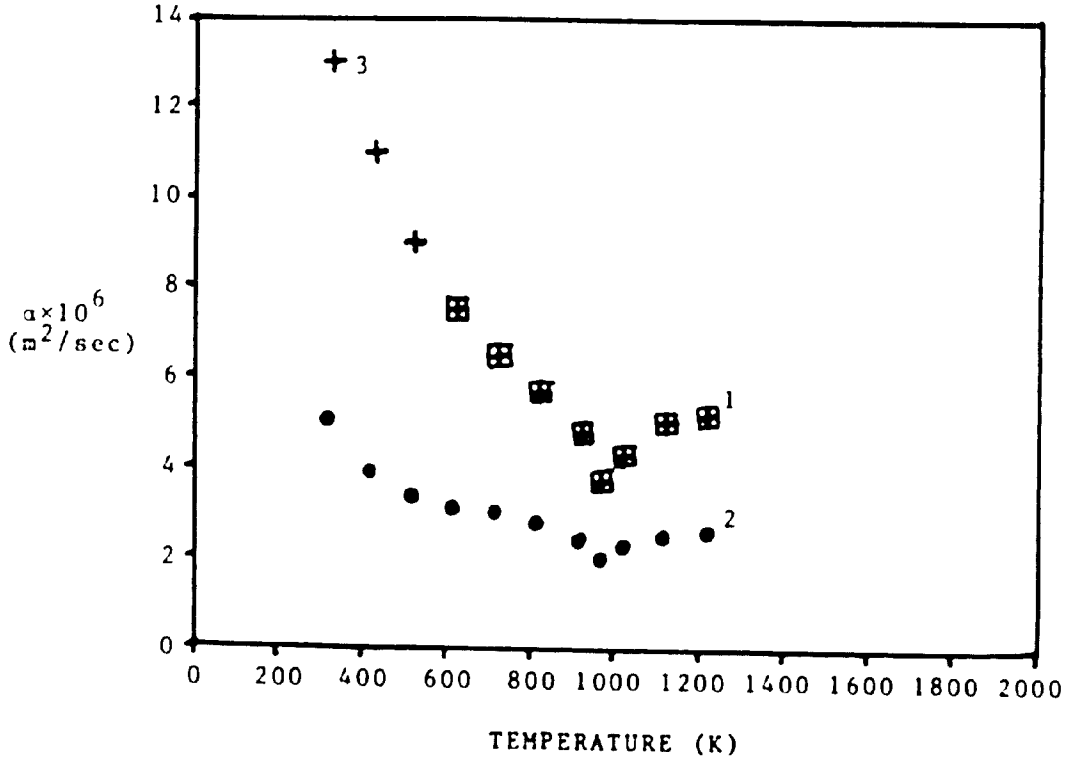

FIGURE B1. Variation of Thermal Diffusivity with Temperature of 1023 Steel Measured by Different Detection Techniques. Curve 1 was measured using the infra-red detector technique. Curve 2 was measured using the thermocouple detection technique with the thermocouple cemented to the sample. Curve 3 was measured using the thermocouple detection technique with the thermocouple spot-welded to the sample.

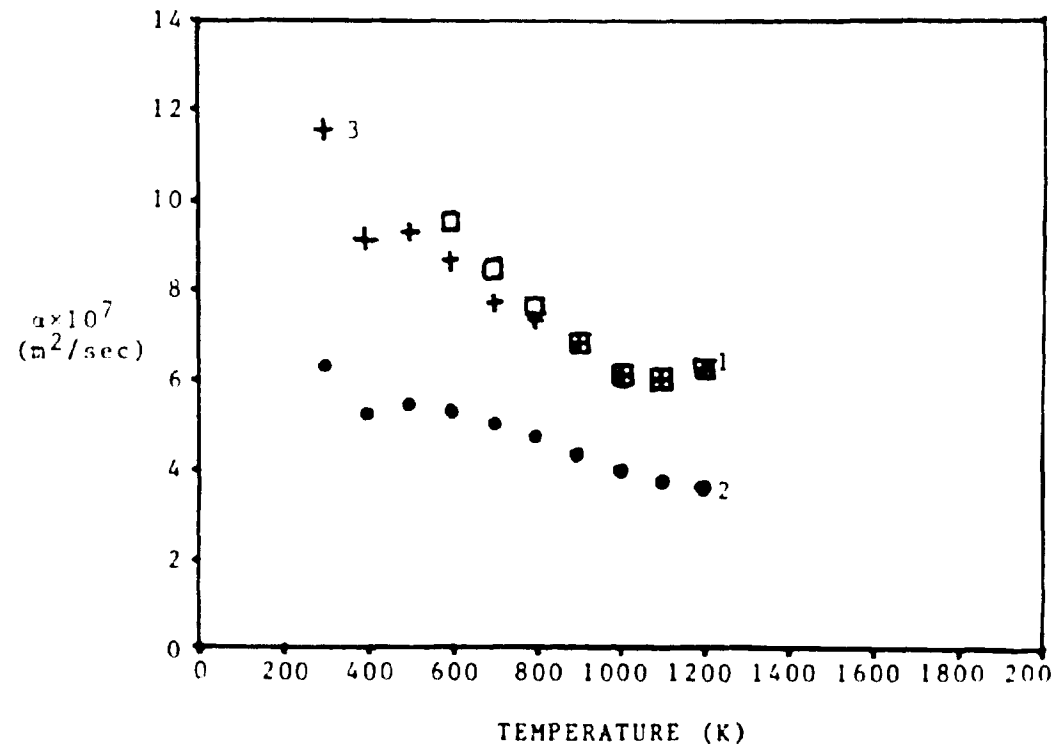

FIGURE B2. Variation of Thermal Diffusivity with Temperature of (MnZn)Fe_2O_4 Measured by Different Detection Techniques. Curve 1 was measured using the infrared detector technique. Curve 2 was measured using the thermocouple detection technique with the thermocouple cemented to the sample. Curve 3 was measured using the thermocouple detection technique with the thermocouple contact made with silver paste before the thermocouple was cemented to the sample.

Curve 3 was generated with the two thermocouple leads spot welded to the back of the sample. By comparing the three curves one can observe two things. First, that Curves 1 and 3 agree quite well. This would imply that they are correct. The second thing one can observe is that the only difference in the experimental parameters between Curves 2 and 3 is the means by which the thermocouple is attached to the sample. This would indicate that the contact between the thermocouple and the sample is not adequate for Curve 2.

Figure B2 shows the results for a sample of $(MnZn)Fe_2O_4$. Curve 1 was measured using the infra-red detector. Curves 2 and 3 were measured using a differential thermocouple. The thermocouple for Curve 3 was attached with silver paste between the thermocouple bead and the sample and then cemented. No silver paste was used for Curve 2. The silver contact for Curve 3 was sintered for two hours at 1000K before measurements were performed. Again the measurement performed with just the thermocouple cemented to the sample, Curve 2, yield lower values of thermal diffusivity than Curves 1 and 3. Curve 3 shows the improved accuracy of the thermocouple technique when a sintered silver contact is used. Another factor to consider is the gauge of the thermocouple wire. If too heavy a gauge of wire is used, the thermocouple can act

as a heat sink and decrease the values measured. Thoughtful caution must be employed whenever a thermocouple measurement technique is used.

Figures B1 and B2 also show the sensitivity of the techniques of thermal diffusivity measurement to changes occurring within a material. In figure B1 the effect of the α-γ phase transition on the thermal diffusivity of the steel sample is shown. Parker, et al, also observed this. In figure B2 the effect of passing through the Curie temperature of the ferrite can be seen. In both cases the distortion of the structure caused by the transition results in a decrease in the thermal diffusivity across a narrow temperature range.

Appendix C

Data from Grain Size Distribution Analysis

Tables C1 through CIV give the data acquired in the grain size distribution analysis. The analysis was performed using an oversize count technique. In the tables the symbol M denotes the size of grain which those counted are greater than. The symbol C denotes the number of particles counted in that size category. The symbol K denotes the percentage of the total that the number C represents.

TABLE CI

Grain Size Distribution Analysis Data for Sample NA

M(μm)	10	30	50	70	90	110	125	150	175	200
C(#)	5242	2744	1688	1191	936	729	601	461	387	309
K(%)	100.	52.3	32.2	22.7	17.9	13.9	11.5	8.8	7.4	5.9

TABLE CII

Grain Size Distribution Analysis Data for Sample NG-I

M(μm)	10	30	50	70	90	110	125	150	175	200
C(#)	3820	2164	1400	1017	750	610	532	411	323	260
K(%)	100.	56.6	36.6	26.6	19.6	16.0	13.9	10.8	8.5	6.8

TABLE CIII

Grain Size Distribution Analysis Data for Sample NG-M

M(μm)	10	30	50	70	90	110	125	150	175	200
C(#)	5020	2557	1648	1172	919	701	610	481	364	316
K(%)	100.	50.9	32.8	23.3	18.3	14.0	12.2	9.6	7.3	6.3

TABLE CIV

Grain Size Distribution Analysis Data for Sample NG-O

M(μm)	10	30	50	70	90	110	125	150	175	200
C(#)	3720	1622	1074	759	603	478	406	314	264	218
K(%)	100.	43.6	28.9	20.4	16.2	12.8	10.9	8.4	7.1	5.9

VITA

Eric J. Minford was born to Mr. & Mrs. Jack H. Minford on February 1, 1954 in Bethlehem, Penna. He received his secondary education at Notre Dame High School, Easton, Pennsylvania, graduating in May, 1972 as a National Merit Finalist. In the Fall of 1972 he entered the Pennsylvania State University, University Park Campus and was awarded a Bachelor of Science Degree in Ceramic Science in May, 1976. While at the University, he was elected to the Pennsylvania chapter of Keramos, a national honorary Ceramics fraternity.

Since July, 1976 he has pursued his graduate education in the Department of Metallurgy and Materials Engineering at Lehigh University, his research being funded through the Chemical Metallurgy Program. He is a student member of the American Ceramic Society and is co-author of one technical publication.